J. Fluid Mech. (1981), *vol.* 104, *pp.* 139–158
Printed in Great Britain

Experiments on heat-stabilized laminar boundary layers in water

By STEVEN J. BARKER
Poseidon Research and
University of California at Los Angeles
AND DOUGLAS GILE
Marine Systems Division, Rockwell International

(Received 28 May 1979)

There has been much recent interest in the stabilization of water boundary layers by wall heating. Calculations based upon linear stability theory have predicted transition Reynolds numbers as high as 200 million for a zero pressure gradient boundary layer over a heated wall. The experiment described in this paper was intended to investigate these predictions. The test boundary layer develops on the inside surface of a cylindrical tube which is 0·1 m in diameter and 6·1 m in length. The displacement thickness is small relative to the tube radius under all conditions of interest. The tube is heated by electrical heaters on the outside wall. The location of transition is determined by flush-mounted hot-film probes, or by flow visualization at the tube exit.

A transition Reynolds number of 15 million has been obtained without heat, which shows that free-stream turbulence and other perturbations are well controlled. A transition Reynolds number of 47 million has been obtained with an 8 °C wall overheat. However, as temperature is further increased there are no additional increases in transition Reynolds number, which is in contradiction to the theory. Several possible reasons for the discrepancy between theory and experiment have been investigated.

1. Introduction

Numerical calculations such as those of Wazzan, Okamura & Smith (1968, 1970) have predicted that wall heating can produce large increases in the transition Reynolds numbers of water boundary layers. The increased stability results from the decrease in fluid viscosity near the wall due to the heating. This increases the curvature of the velocity profile near the wall, making the flow more stable to small disturbances. The present study is an experimental investigation of these predictions, using the boundary layer developing on the inside wall of a cylindrical tube. This boundary layer is thin relative to the tube diameter, so that it approximates a boundary layer over a flat plate at zero angle of incidence.

Calculations of wall heating effects are based upon linear, two-dimensional stability theory. The mean flow in the boundary layer is assumed plane and parallel, and the superposed small disturbance is described by a stream function

$$\psi(x,y,t) = \phi(y)e^{i\alpha(x-ct)}. \tag{1}$$

0022–1120/81/4652-3520 $02.00

In this equation, x and y are the usual boundary-layer co-ordinates, ϕ is the amplitude of the disturbance, α is the wavenumber and is assumed real, and c is the phase velocity which may be complex. The sign of the imaginary part of c determines whether the disturbance is temporally amplified or damped. From here the analysis parallels the derivation of the Orr–Sommerfeld equation. The stream function is substituted into the Navier–Stokes equations, which are then linearized. However, in this case the variation of fluid properties with the y co-ordinate must also be accounted for. It is assumed that in water the most important variable fluid property is viscosity, which is a function only of the local fluid temperature T. It is further assumed that T is a function of y only, meaning that we neglect the effects of the disturbance upon the temperature profile. The resulting equation for the non-isothermal water boundary layer is known as the 'modified Orr–Sommerfeld equation'

$$(U-c)(\phi''-\alpha^2\phi)-U''\phi = \frac{-1}{\alpha Re}[\mu(\phi''''-2\alpha^2\phi''+\alpha^4\phi) + 2\mu'(\phi'''-\alpha^2\phi')+\mu''(\phi''+\alpha^2\phi)]. \quad (2)$$

Here $U(x)$ is the external flow velocity, and Re is the Reynolds number based upon free-stream velocity U_∞ and boundary-layer thickness δ. Primes indicate differentiation with respect to x. This equation differs from the usual Orr–Sommerfeld equation by the addition of the two variable viscosity terms, containing μ' and μ''.

Wazzan *et al.* (1968) have solved (2) numerically for the boundary layer over a heated flat plate, using non-isothermal velocity profiles generated by the method of Kaups & Smith (1967). The solutions determine the 'critical' Reynolds number, which is the lowest Reynolds number at which any small disturbance has a positive amplification rate. The last step of the calculation is to relate this critical Reynolds number to the transition Reynolds number, using the 'e to the ninth' method of A. M. O. Smith (1957). According to this empirical criterion, transition occurs when the most unstable disturbance has grown to e^9 (which is 8103) times its original amplitude. The linear theory is used in calculating the growth of the disturbance to this amplitude.

Strazisar, Prahl & Reshotko (1977) have measured growth rates of small disturbances generated by a vibrating ribbon in a heated boundary layer. They established neutral stability curves and were able to determine critical Reynolds numbers for wall overheats of up to 2·8 °C. (5 °F). They found that in this range of overheats, critical Reynolds numbers are in reasonable agreement with theoretical predictions. These experiments did not yield data on transition, or on stability at higher overheats.

The Wazzan *et al.* (1970) calculations predict that the transition Reynolds number of a zero pressure gradient boundary layer should increase with wall temperature up to about 40 °C (70 °F) of overheat for a free-stream temperature of 16 °C (60 °F). At that overheat, the predicted transition Reynolds number is approximately 200 million. This Reynolds number is based upon free-stream velocity and distance from the leading edge. Thus the experiment designed to investigate wall heating effects must generate a very high-Reynolds-number boundary layer while maintaining low free-stream disturbance levels. The wall should be very smooth and its temperature precisely controlled. These are the chief considerations that led to the experimental geometry described below.

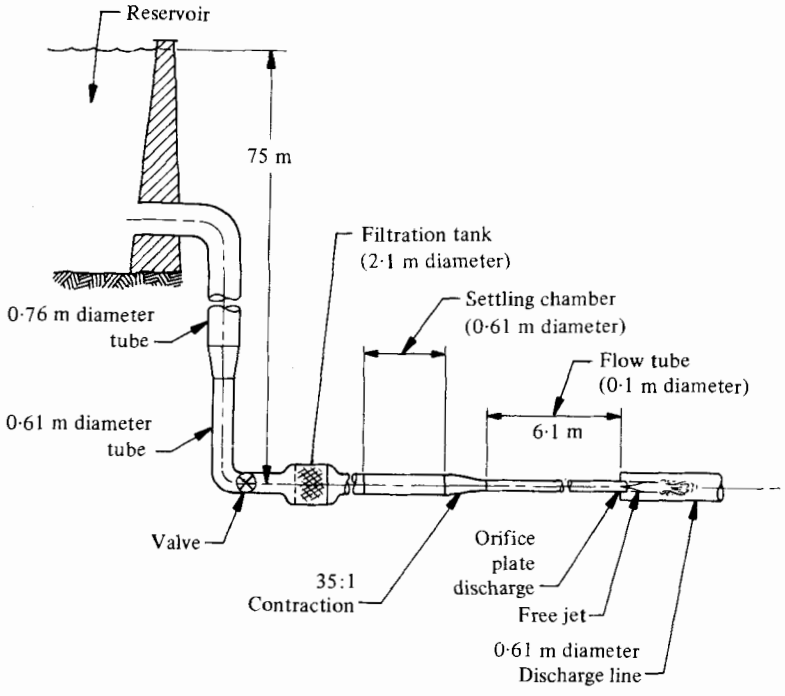

FIGURE 1. Flow tube experimental geometry.

2. Experimental apparatus

2.1. *Configuration*

A facility in which water is recirculated through the test section was avoided for two reasons. (1) Heat is continuously added to the test section so that a recirculating experiment would require a heat exchanger to establish constant free-stream temperature. (2) The free-stream turbulence level in the test section should be less than 0·05 per cent, which has previously been difficult to achieve in a closed circuit water facility. The experiment must therefore be of the 'blow-down' type, in which water is removed from one reservoir and discharged into another. Run times of more than twenty minutes were desired, which led to the selection of the Colorado State University Engineering Research Centre as the site of the experiment. Here the water supply is Horsetooth Reservoir, which provides water to the laboratory through a 0·6 m diameter pipe at a total pressure of 6.8×10^5 N/m^2 (100 lb/in.^{2}) without the use of pumps. The discharge flows into a smaller lake below the laboratory. At the maximum flow rate of this experiment (200 l/s), the run time is effectively unlimited.

The experimental apparatus includes a settling chamber for turbulence management, a contraction section, a flow-tube test section and various types of instrumentation described below. A diagram of the experimental geometry is shown in figure 1.

2.2. *Turbulence management*

The inside diameter of the settling chamber is 0·6 m, the same as that of the supply line from the reservoir. The test section is 0·102 m in diameter, which results in a

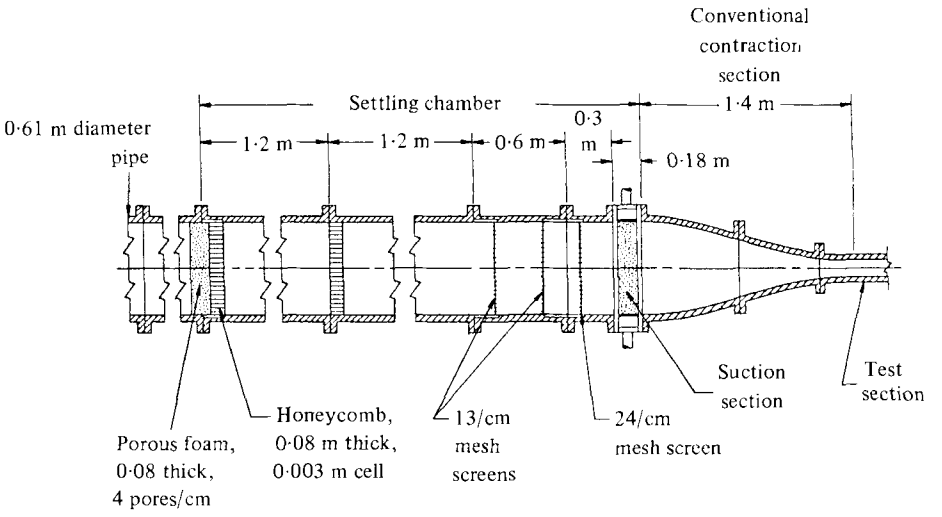

FIGURE 2. Settling chamber and 'conventional' contraction.

contraction ratio of 35 : 1. The settling chamber is 3·35 m long and is made up of four separable sections, as shown in figure 2. The sections are made of fibreglass to avoid heat transfer through the walls. Both ends of each section are counter-bored to hold a 0·15 m long aluminium cylinder with a 1·3 cm wall thickness. Each cylinder may contain one or more turbulence manipulators, including wire screens, porous foam, or honeycomb material. This design allows the settling chamber to be assembled in different configurations and optimized experimentally.

The details of the design and optimization of the turbulence management system are reported separately (Barker 1978). The configuration shown in figure 2 was arrived at after considerable testing. There is a large body of literature on the subject of turbulence management, which provided some guidelines for the optimization of the present system. The most detailed recent study is that of Loehrke & Nagib (1972), who measured mean velocities and turbulence levels downstream of various turbulence manipulators. Recommendations for the construction of a turbulence management system have also been given by Corrsin (1963), Bradshaw (1965), and Lumley & McMahon (1967).

At the downstream end of the settling chamber there is a short section containing porous wall boundary-layer suction (figure 2). Hot-film anemometer surveys in the settling chamber have shown that at test-section velocities above 9 m/s, the settling-chamber boundary layer becomes turbulent before the flow enters the contraction. A thin turbulent boundary layer entering the strong favourable pressure gradient of the contraction section will tend to 'relaminarize' as described by Launder (1964) and Back, Cuffel & Massier (1969). However, relaminarization would leave us with unknown initial conditions at the test-section entrance. Therefore we added the suction section to remove completely the turbulent boundary layer. This section contains a 0·1 m length of porous wall surrounded by an annular plenum chamber. The suction flow from the plenum is controlled by a valve and measured by a Venturi meter. At each test-section velocity above 9 m/s, the suction is adjusted

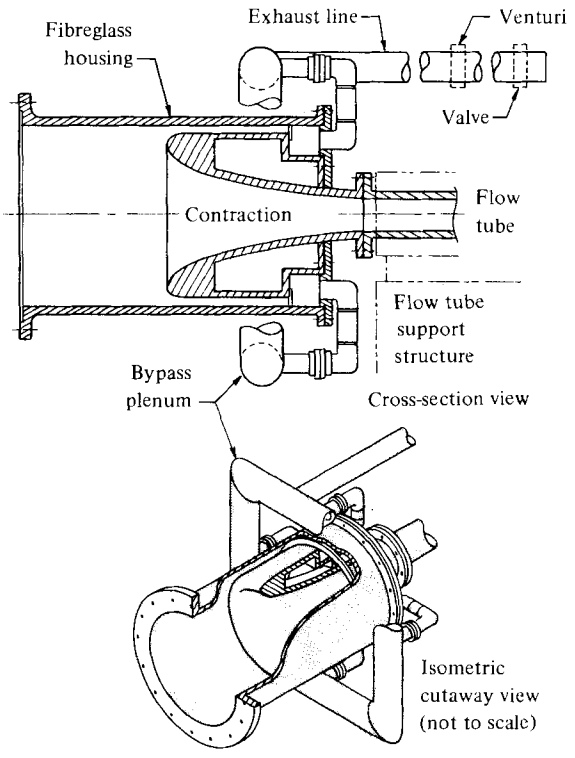

FIGURE 3. Bell-mouth contraction section.

to the minimum value necessary to remove the turbulent boundary layer at the contraction entrance. This adjustment is discussed further in § 3.1.

2.3. *Contraction and test section*

Two different contraction sections have been used in this experiment. The first is a 'conventional' contraction (figure 2), designed by potential-flow calculations using the method of Chmielewski (1974). This contraction is 1·37 m long, with a length-to-diameter ratio of 2.25. It is constructed in two sections: a fibreglass upstream half and an aluminium downstream half. The joint between the two sections is in the region of strongest favourable pressure gradient, and has no measurable step across it.

The second contraction section was designed to avoid the Goertler instability (Schlichting 1968) that occurs in the concave wall region of the conventional contraction. The entrance of this contraction is a fully convex curved 'bell-mouth' shape, surrounded by an annular bleed flow which removes the settling chamber boundary layer, as shown in figure 3. The bell-mouth contains no region of concave streamwise wall curvature, and thus has no tendency to generate Goertler vortices. The porous wall boundary-layer suction section is not needed with the bell-mouth contraction.

The flow-tube test section is 6·4 m in length and 0·102 m in diameter, with a 2·5 cm wall thickness. It is made of aluminium, and the inside wall has been polished to a surface roughness of less than 10^{-7} m r.m.s. (4 micro-inches). Surface waviness has

been measured as less than one part per thousand for wavelengths less than 2 cm. The tube has been optically aligned on site so that it is straight to within less than 0·018 cm over its entire length. The outside wall is covered with electrical band heaters, which are connected together in groups covering 0·3 m of length. Each heater group is controlled by a servo-system which maintains a preset temperature on a thermocouple located near the inside tube wall. In this way the inside wall temperature can be controlled independently of flow velocity, and different variations of temperature along the tube length can be studied.

To avoid tripping the boundary layer, there are no penetrations of the inside tube wall except at the downstream end. An array of thermocouples is imbedded within the wall, at various locations along the tube length. At each location there is one thermocouple on the outside surface and one in a small hole drilled to within 0·15 cm of the inside surface. The temperature difference between these two thermocouples determines the heat flux through the wall. Since heat flux increases by a factor of about ten at the transition point, these temperature measurements can provide a good transition indicator. A total of 53 thermocouple voltages are digitized and recorded.

In addition to the heat flux measurements, two other methods can be used to determine transition at the downstream end of the tube. First, there is a short instrumented section which can be added to the end of the test section. This section is 0·61 m long and its inside diameter matches that of the test section to within 2×10^{-5} m. The instrumented section contains eight flush-mounted hot-film anemometers which can determine whether the boundary layer over the probe is laminar or turbulent at any time. The intermittency, defined as the fraction of time during which the boundary layer is turbulent, can thus be found at each probe location. The instrumented section can also be used to survey the boundary layer with a traversing Pitot tube. The boundary layer is less than 0·5 cm thick, and the Pitot tube cross-section is correspondingly small: $0{\cdot}013 \times 0{\cdot}076$ cm. The smaller dimension is oriented in the direction perpendicular to the wall. The Pitot tube is traversed from the wall to the free stream with a micrometer gauge whose uncertainty in position is less than 0·002 cm. Furthermore, the central portion of the instrumented section can be rotated azimuthally so that the Pitot tube can be traversed about the circumference. This rotation can be performed while the experiment is running.

The second method of determining transition at the downstream end involves flow visualization. The flow tube test section terminates in a nozzle, whose pressure drop controls the static pressure in the test section for a given velocity. This static pressure must be maintained high enough to avoid cavitation or outgassing from the heated walls. The water is discharged from the nozzle as a free jet into air. This geometry minimizes the propagation of disturbances from the turbulent downstream flow into the test section. In the early flow tube experiments, the exit nozzle was simply a sharp-edged orifice plate at the end of a 1 m extension tube added to the heated test section. Concern over disturbances generated upstream of this orifice plate led to the development of a smooth contraction 0·2 m in length to replace the orifice plate. With this smooth contraction, a laminar boundary layer can be maintained all the way into the exit jet. Transition can then be determined simply by the appearance of the exit jet, as shown in figure 4. For the laminar boundary layer of figure 4*a*, note the glassy appearance of the exit jet near the nozzle. The effects of test section exit conditions upon transition will be discussed in more detail below.

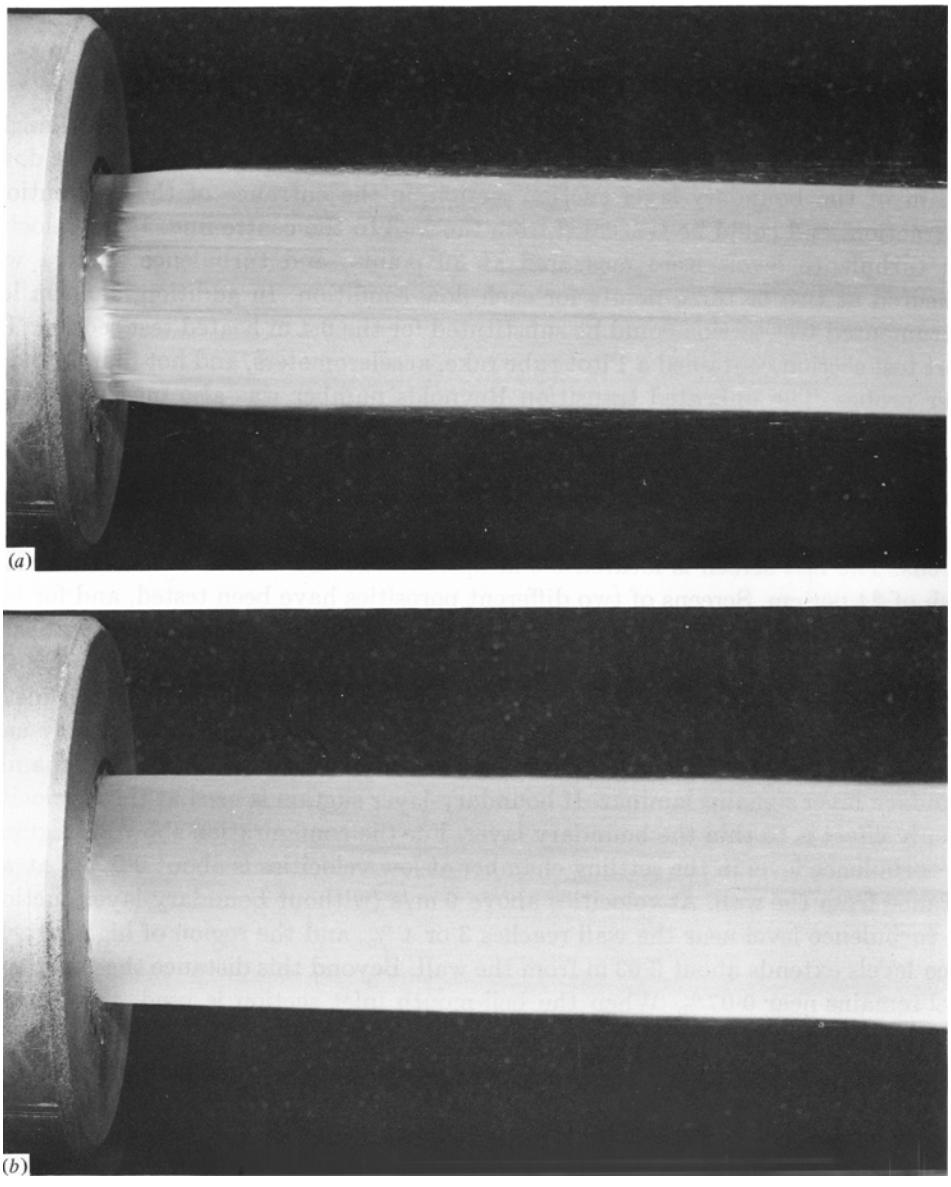

FIGURE 4. Flow tube exit jet: (a) laminar boundary layer; (*b*) turbulent boundary layer.

As a variation on the smooth contraction exit, a 'plug nozzle' has also been developed. This consists of a strut-supported central cone (30 ° apex angle) which can be moved axially in and out of the end of the test section. This adjustment permits us to vary the discharge coefficient of the nozzle, thus varying the test section static pressure for a given flow velocity. The plug nozzle can also maintain a laminar boundary layer all the way to the exit jet in the same way as the smooth contraction nozzle. With any of these exit configurations, the test section velocity can be determined from the stagnation pressure measured in the settling chamber, and the known discharge coefficient of the nozzle.

3. Results

3.1. *Free-stream turbulence*

Mean and fluctuating velocities were measured in the settling chamber by a cylindrical hot-film anemometer. The probe penetrated the settling chamber wall 0·1 m downstream of the boundary-layer suction section, in the entrance of the conventional contraction, and could be traversed from the wall to the centre-line. Mean velocities and turbulence levels were measured at 30 points, and turbulence spectra were measured at two or three points for each flow condition. In addition, a 1·2 m long instrumented test section could be substituted for the 6·4 m heated test section. This short test section contained a Pitot rube rake, accelerometers, and hot film boundary layer probes. The unheated transition Reynolds number was also measured in the 1·2 m tube for each settling chamber configuration. This Reynolds number varied from 800000 for the empty settling chamber with no turbulence manipulators to 5·0 million for the 'best' configuration. This configuration, which is shown in figure 2, includes one piece of porous polyurethane foam, two sections of honeycomb, and three screens. The last screen is located 0·3 m upstream of the suction section, and has a mesh of 24 per cm. Screens of two different porosities have been tested, and for both cases the porosity is equal to or greater than the 57 % open area criterion established by Bradshaw (1965).

Detailed results of the measurements in the settling chamber and 1·2 m instrumented tube have been reported separately (Barker 1978), and will be only summarized here. At test-section velocities of less than 9 m/s, the settling chamber boundary layer remains laminar. If boundary-layer suction is used at these velocities its only effect is to thin the boundary layer. For the configuration shown in figure 2, the turbulence level in the settling chamber at low velocities is about 0·07 % at any distance from the wall. At velocities above 9 m/s (without boundary-layer suction), the turbulence level near the wall reaches 3 or 4 %, and the region of higher turbulence levels extends about 0·03 m from the wall. Beyond this distance the turbulence level remains near 0·07 %. When the bell-mouth inlet section is used, this layer of turbulent fluid is removed entirely by the bleed flow. With the conventional contraction section, the porous-wall boundary-layer suction must be used to remove the turbulent fluid. The suction rate is adjusted to the minimum value required to remove a 3 cm layer of fluid at the given flow velocity. Velocity surveys have shown that this suction rate produces minimum turbulence intensity near the settling-chamber wall.

The settling-chamber velocity measurements and unheated transition Reynolds numbers in the 1·2 m tube indicate that the turbulence management system is performing well. If the turbulence level reduction through the contraction is proportional to the square root of the contraction ratio (Pankhurst & Holder 1952), then the turbulence level in the test section should be about 0·01 %. This is lower than the turbulence levels recorded in most wind tunnels, and much lower than those of previously reported water tunnels.

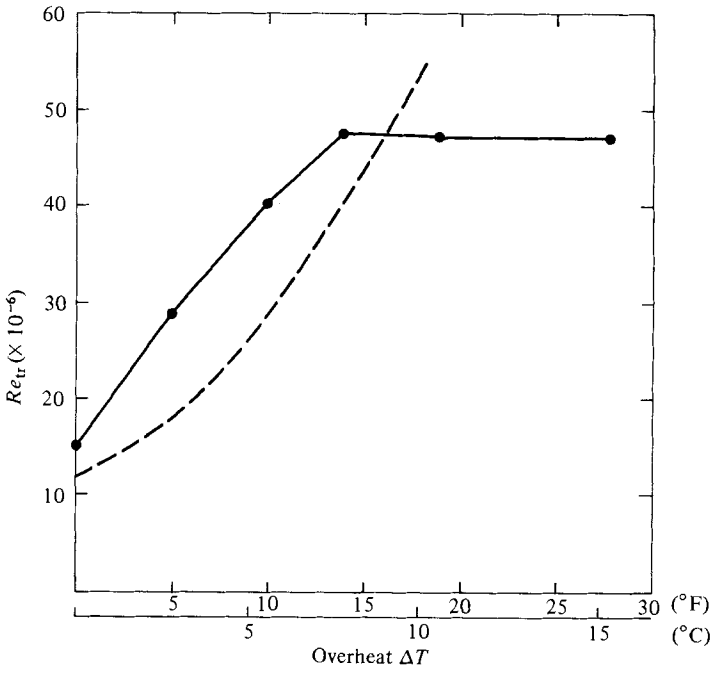

FIGURE 5. Transition Reynolds number versus wall overheat: 'best' results and theory. ●—●, flow tube; ---, Wazzan *et al.* (1968), $\beta = 0{\cdot}07$.

3.2. *Maximum transition Reynolds numbers: Comparison with theory*

Figure 5 shows measured transition Reynolds numbers in the 6·1 m heated test section as a function of overheat for the uniform wall temperature case. The results shown here are the highest Reynolds numbers that have been obtained in the experiment, after two years of testing and modifying the apparatus. (The sequence of modifications and their effects will be discussed below.) These results were achieved using the smooth exit nozzle shown in figure 4 with transition occurring at the exit, as determined by flow visualization. The bell-mouth entrance section (figure 3) was used, with the bleed flow rate adjusted to maximize the transition Reynolds number. This optimum bleed flow results in approximately one-third of the settling-chamber flow volume passing through the bypass.

The Reynolds numbers in figure 5 are based upon the test-section entrance velocity, the length of the tube from the 'nose' of the bell-mouth inlet to the exit nozzle, and the free-stream kinematic viscosity at the measured free-stream temperature. The water temperature was approximately 10 °C during these tests. Note that the transition Reynolds number obtained with no heat is 15 million. As wall heat is increased from zero, the Reynolds number increases rapidly to a maximum value of 47·5 million at 8 °C overheat. Additional increases in wall temperature do not further increase the transition Reynolds number. In earlier flow-tube results (Barker & Jennings 1977) it was also shown that non-uniform wall temperature (for example, ΔT proportional to $x^{\frac{1}{2}}$) does not increase the maximum transition Reynolds number.

To compare these flow-tube results directly with theory, we must account for the favourable pressure gradient resulting from the boundary-layer displacement effect

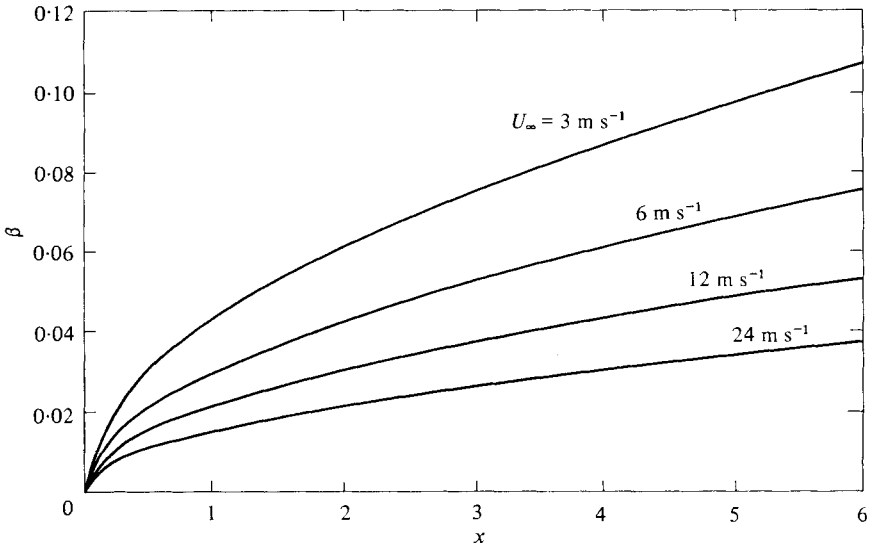

FIGURE 6. Pressure gradient parameter β versus x in the flow tube.

in the tube. The usual way to characterize the streamwise pressure gradient in a boundary layer is by the similarity parameter β (Schlichting 1968). For the general class of wedge flows, the external velocity ($U(x)$ is given by $U = Cx^m$, and β is equal to $2m/(m+1)$. Both m and β are independent of x for wedge flows, and both equal zero for a flat plate at zero angle of incidence. For the flow tube we have calculated approximate local values of β, using the Blasius formula for the boundary-layer displacement thickness:

$$\delta^* = 1{\cdot}72\,(\nu x/U_\infty)^{\frac{1}{2}}. \tag{3}$$

This calculation has also been iterated to include the effect of favourable pressure gradient upon δ^*, but the effect of this upon β is negligible. Calculated values of β as a function of x at several values of U_∞ are shown in figure 6. β is proportional to the square root of x, and thus has its largest value at the downstream end of the tube.

Although the published calculations of Wazzan *et al.* (1968, 1970) are for the zero pressure gradient case, some results for small positive β have been computed (Wazzan, private communication). The effect of positive β, or favourable pressure gradient, is to increase the transition Reynolds number for a given overheat. The predicted transition Reynolds numbers for $\beta = 0{\cdot}07$ are shown as the dashed curve in figure 5. Note that this curve is for a constant positive β, while in the flow tube the local value of β varies with both x and U_∞ as shown in figure 6. The value of 0·07 was selected as being an average value for the tube in the velocity range of interest. However, β in the tube will be greater than 0·07 at low velocities, which may explain why the experimental points lie above the predicted curve at overheats below 8 °C.

The most significant difference between theory and experiment is the fact that the experimental curve levels off abruptly at a transition Reynolds number of 47·5 million, while the predicted curve continues to rise with an increasing slope, reaching a maximum of over 200 million at 40 °C overheat. There are several possible reasons for this disparity at the higher overheats.

(1) The theory does not account for the destabilizing effects of density stratification, which become increasingly important as overheat is increased. Buoyancy effects can destabilize the boundary layer in three ways: (*a*) the bottom-wall boundary layer is unstably stratified, and is subject to thermal convection rolls, similar in form to Goertler vortices; (*b*) the side-wall boundary layer has a cross-flow velocity component due to the rising fluid near the wall; and (*c*) the top-wall boundary layer grows in thickness faster than normal because of the fluid rising up from the sides. These mechanisms have been investigated in further experiments which will be discussed below.

(2) The theory relies on the 'e^9 criterion' to predict transition. This criterion has never before been applied to boundary layers with inhomogeneous physical properties (i.e. variable viscosity). It does not account for the intensity or frequency spectrum of free-stream turbulence. Linear growth of small disturbances is assumed over a Reynolds-number range of more than 50 million for this experiment.

(3) Finite wall roughness is neglected by the theory. The importance of roughness will increase with increasing overheat or flow velocity because of the resulting thinning of the boundary layer. Roughness that is insignificant at a low overheat may thus become important as overheat increases. The surface of the flow tube has been kept as smooth as possible. Profilometer measurements have shown that the surface roughness is less than 10^{-7}m (4 micro-inches) r.m.s.

(4) The theory has assumed a flat plate in a uniform free-stream flow, while the geometry of the flow tube is somewhat different. For example, the free stream is fully bounded by the walls in the experiment, and these walls have curvature in the direction transverse to the flow. The ideal flat-plate geometry has an unbounded free stream and no wall curvature.

(5) The theory neglects possible effects of impurities, such as suspended particulates in the free stream.

The remainder of the flow tube study has been directed toward understanding the differences between predicted and measured transition Reynolds numbers. We have investigated specifically the effects of geometric differences, buoyancy, and particulate contamination of the free stream.

3.3. *Effects of tube geometry: exit conditions*

The first effect of experimental geometry discovered in the flow tube was the fact that the highest transition Reynolds numbers are obtained when the full length of the test-section boundary layer is laminar. Transition Reynolds numbers are thus determined by slowly increasing the flow velocity until the flow at the tube exit becomes intermittently laminar and turbulent. (A criterion of 30 % intermittency has been arbitrarily adopted as defining transition in this experiment.) If the flow velocity is further increased, so that the transition region moves upstream in the test section, the transition Reynolds number will rapidly decrease. We can determine the location of transition in this case by heat flux measurements, as shown in figure 7. Here we see a very sudden increase in the temperature change between the inside and outside surfaces of the tube wall at the location of transition, where the boundary-layer heat flux increases roughly by a factor of 10. Note that the inside wall temperature is held nearly constant by the temperature control system.

The fact that transition Reynolds number depends upon flow velocity could be a

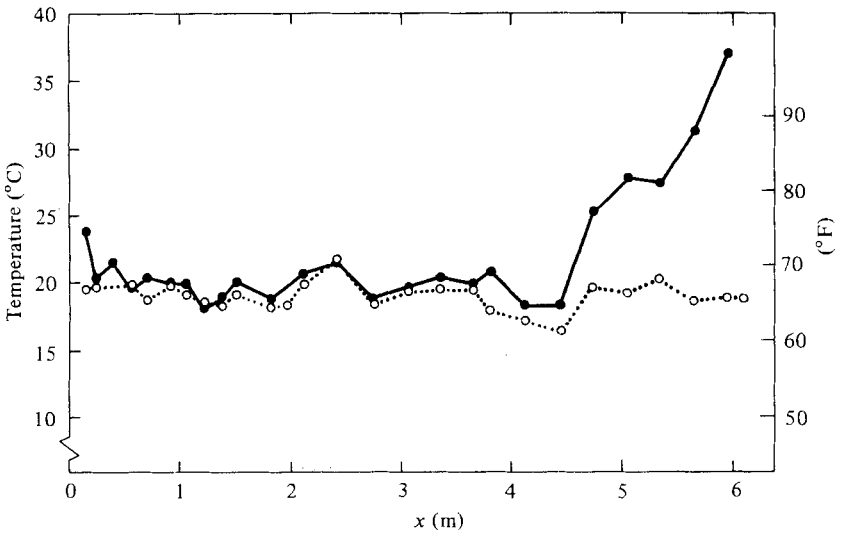

FIGURE 7. Wall temperature measurements showing increase in heat flux at transition. ●—●, external wall temperature; ○···○, internal wall temperature.

result of the experimental geometry. The free stream in the flow tube is confined by the boundary layer, and can thus be affected by the boundary layer once the latter becomes turbulent. The resulting fluctuations in the free-stream velocity could destabilize the boundary layer upstream of the turbulent region and thereby reduce the transition Reynolds number.

To test the hypothesis of downstream disturbances affecting transition Reynolds number, we have conducted a study of the dependence of transition upon tube exit geometry. As noted above, there are three types of exit nozzle available: orifice plates, the smooth contraction, and the plug nozzle. In addition, the length of unheated straight tube between the heated section and the exit can be varied from zero to 3·7 m in increments of 1·22 m. For each configuration, transition can be determined either at the exit itself or at the end of the heated section. Transition at the exit is easily determined by flow visualization, as shown in figure 4. This visual diagnostic works equally well for the plug nozzle, and somewhat less well for the orifice plate exit. The smooth contraction of figure 4 imposes a favourable pressure gradient on the boundary layer near the exit, which increases the stability of the boundary layer in that region. However, the nozzle itself is only 0·2 m long, and that length is not included in the transition-Reynolds-number calculation. Thus the exit nozzle pressure gradient has no effect upon the results.

A typical comparison of data for different exit nozzles is shown in figure 8. The conventional contraction and porous-wall boundary-layer suction were used in this test. The results of figure 8 were obtained with one 1·22 m extension tube on the end of the test section, followed by either the orifice plate or the smooth contraction nozzle. Transition was determined at the exit in both cases. Note that the transition Reynolds numbers with the smooth contraction nozzle are about 20 % higher than those with the orifice plate. If a longer length of unheated extension tube (2·44 m) is placed between the test section and the exit, the difference between these two exit

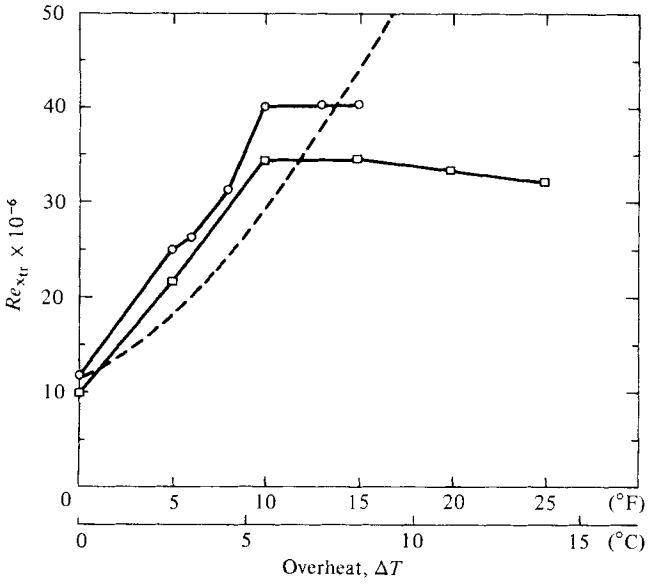

FIGURE 8. Effect of exit nozzle upon transition Reynolds number: orifice plate and smooth contraction nozzle. ○—○, smooth nozzle; □—□, orifice plate; ---, Wazzan *et al.* (1968), $\beta = 0{\cdot}07$.

nozzles is greater. The transition Reynolds numbers with the smooth exit are about the same as in figure 8, while those with the orifice plate are reduced by about 30 %. This is attributed to the fact that the laminar boundary layer at the end of a longer length of unheated tube is less stable, and is thus more sensitive to the disturbances created by the orifice plate exit. If the unheated extension length is increased still further to 3·66 m, the transition Reynolds numbers at the exit are lower than in figure 8 even with the smooth contraction nozzle. This demonstrates the destabilizing influence of the unheated wall downstream of the heated test section.

Transition Reynolds numbers obtained with the plug nozzle exit have been essentially the same as those with the smooth contraction nozzle for all test geometries. This is a logical result since both of these nozzles can maintain a laminar boundary layer all the way into the exit jet.

If transition is determined at the end of the heated section rather than at the exit itself, the influence of the nozzle geometry is much less pronounced. This leads to the conclusion that while the exit boundary conditions can affect the transition process near the exit, this influence does not propagate far upstream. The best comparison with theory can be expected for a laminar exit flow, since in this case there is no time-dependent interaction between the boundary layer and the free stream.

3.4. *Effects of tube geometry: entrance conditions*

Perhaps the most significant difference between the flow tube and a flat plate in a uniform free stream is that the flow tube has no leading edge. In the case of the conventional contraction section, the test boundary layer originates at the downstream end of the porous-wall suction section. This boundary layer is then subjected

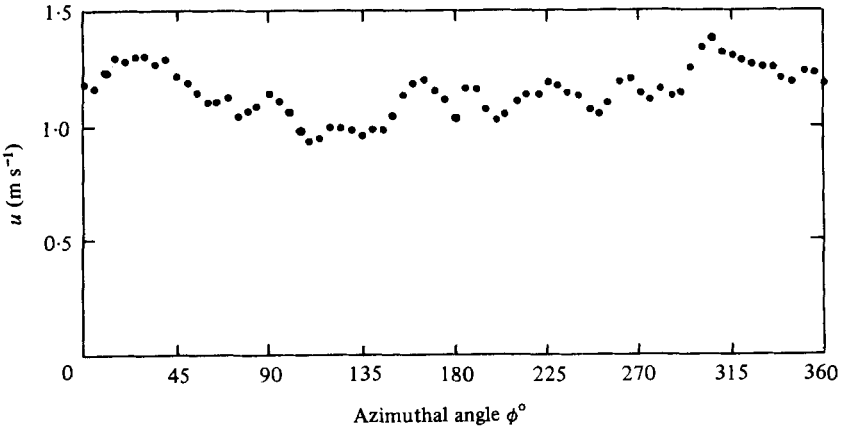

FIGURE 9. Azimuthal velocity profile at exit: u versus ϕ at $y = 0{\cdot}005$ m, $U_\infty = 1{\cdot}5$ m/s.

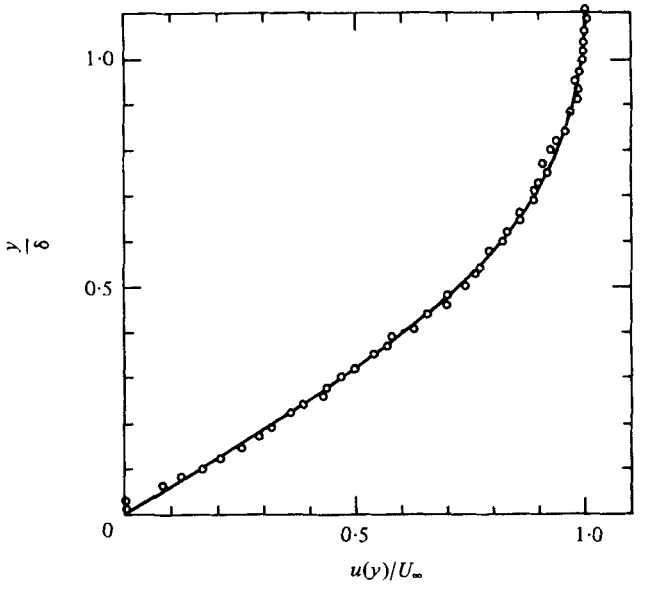

FIGURE 10. Boundary layer profile: u/U_∞ versus y/δ, $U_\infty = 1{\cdot}5$ m/s, no heat, $\phi = 90°$. The solid line is the Blasius profile.

to a strong favourable pressure gradient and streamwise wall curvature in both directions before it enters the constant diameter test section. It was assumed in the original design that the favourable pressure gradient of the contraction would greatly thin the boundary layer and thus eliminate any dependence upon the flow upstream of the test section. When boundary-layer velocity profiles at the downstream end of the flow tube were obtained with the instrumented section, this assumption became questionable. Figure 9 shows a mean velocity profile obtained without heat, in which the Pitot tube is held at a fixed distance from the wall (0·005 m) while the instrumented section is rotated azimuthally. The wave-like

dependence of the velocity upon the azimuth angle ϕ is a result of significant azimuthal variations of the boundary layer thickness. Velocity profiles of the form u versus y (distance from the wall) have also been measured. A typical example of a normalized profile is shown in figure 10, compared with the theoretical (Blasius) profile. Such profiles have been measured at several azimuth angles, and the boundary-layer thickness is found to vary by as much as 50 % over the tube circumference. However, the thickness averaged over the circumference is almost exactly what is predicted by two-dimensional theory. This result is independent of test-section velocity or wall overheat.

Since these azimuthal waves are not a buoyancy effect (they occur with no heat), it seems reasonable to assume that they originate from the upstream end of the tube. Their form suggests the presence of streamwise vortices in the boundary layer, a hypothesis which is supported by the fact that the waves are more closely spaced at higher velocities. We therefore surmised that the streamwise vortices are created by the Goertler instability (Schlichting 1968) in the concave-curved portion of the contraction section. Once generated, these vortices would not be removed by the favourable pressure gradient of the contraction, nor would they diffuse into the wall by the action of viscosity.

These results led to the development of the 'bell-mouth' inlet section, shown schematically in figure 3. This inlet contains no region of concave streamwise wall curvature, so the boundary layer should not be subject to a Goertler instability. There has been conjecture about the possibility of Goertler vortex formation near a forward stagnation point, but a recent investigation of this possibility has produced negative results (Wilson & Gladwell 1978). The shape of the bell-mouth inlet was designed to maintain continuity of the first three derivatives of the wall coordinate. The width of the annular gap around the outside of the bell-mouth (0·025 m) was chosen so that about twice the thickness of the settling chamber boundary layer would be removed by the bleed flow when the stagnation point is located on the nose of the inlet. Since the nose is quite rounded in this case, there is some flexibility in adjusting the location of the stagnation point. This adjustment is made by varying the ratio of the volume flow through the test section to that through the bleed flow.

The experimental results using the bell-mouth inlet section are similar to those of the conventional contraction. The maximum transition Reynolds number was increased from 42 to 47·5 million with the change in contractions, an improvement of 13 %. In fact, this change appears to be partially the result of an improvement in the settling chamber screens rather than the change of inlets. The most surprising fact is that the 'waves' in the azimuthal velocity profiles are still present with the bell-mouth inlet, with roughly the same wavelengths and amplitudes as before. The conclusion of this comparison is that these waves are not the result of Goertler vortices generated in the concave region of the conventional contraction.

Once it was determined that the change in the geometry of the inlet had only a small effect upon both transition Reynolds numbers and mean velocity profiles, possible sources of streamwise vorticity in the settling chamber were considered. A systematic series of changes in the turbulence management system was performed, and the effects of each change upon the azimuthal velocity profiles were measured. These changes included 180° azimuthal rotations of each turbulence manipulator (screens, foam, and honeycomb), and removal of turbulence manipulators, one or

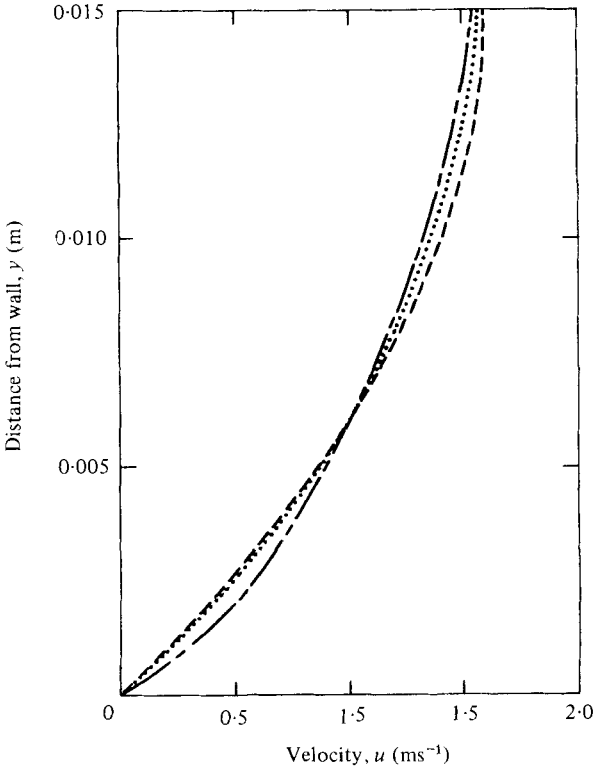

FIGURE 11. Velocity profiles u versus y on bottom wall, showing effects of overheat. $U_\infty = 1{\cdot}5$ m/sec, $\phi = 180°$. ---, $\Delta T = 0°$; ....., $\Delta T = 5°$; – – –, $\Delta T = 10°$

two at a time. If more than two manipulators are removed from the settling chamber, it is impossible to obtain laminar flow at the downstream end of the test section at the velocities of interest. The results of these settling chamber variations were entirely negative. The wave pattern of the azimuthal velocity profile does not rotate when any or all turbulence manipulators are rotated, and neither the wavelength nor amplitude is affected by removal of individual devices. The origin of these three-dimensional disturbances is still a mystery, although similar perturbations in two-dimensional or axisymmetric boundary layers have apparently been observed by several other investigators (Wilson & Gladwell 1978).

3.5. *Effects of buoyancy*

Geometrical differences between the present experiment and the flow over a flat plate apparently do not explain the failure of the theory to predict transition at the higher overheats. Another perturbation that is neglected by the theory is the effect of buoyancy upon the flow. Buoyancy effects have been studied in the flow tube and the results will be summarized here.

As stated above, buoyancy can destabilize the flow-tube boundary layer in three distinct ways. Two of these mechanisms, vortices on the bottom wall and thickening of the top-wall boundary layer, should produce measurable changes in boundary-layer velocity profiles. The third mechanism, cross-flow in the side-wall boundary

layer, should also be accompanied by a thickening of the top-wall boundary layer. The measurement of these buoyancy-induced asymmetries of the velocity field were the original purpose of the 0·61 m instrumented section.

Both u versus ϕ and u versus y profiles have been measured at various overheats for free-stream velocities of 1·5 and 3 m/s. Effects of buoyancy should be greatest at low velocities and high overheats. As mentioned above, wall heat has no discernible effect upon the azimuthal (u versus ϕ) velocity profiles. Figure 11 shows three u versus y profiles at the bottom wall ($\phi = 180°$) for a free-stream velocity of 1·5 m/s at different overheats. The data points have been eliminated for clarity, but they would be distributed about the smooth curves as in figure 10. This particular comparison shows the largest effect of heat upon velocity profiles that has been observed. The effect at higher velocities is not measurable. In fact, the day-to-day variations of the profiles, due apparently to a slight shifting in the positions of the azimuthal waves, are greater than the differences seen in figure 11. The three profiles in figure 11 were all taken within a ten minute period with no changes in the experiment other than the wall temperature.

The primary effect of heating shown in this figure is an increase in the curvature of the profile near the wall. This is not a buoyancy effect; it is the effect of reduced viscosity near the wall, which is the mechanism of boundary layer stabilization. Plots of boundary-layer displacement and momentum thickness versus overheat at various azimuthal angles also show no measurable buoyancy effect. However, the shape factor H (the ratio of displacement to momentum thickness) consistently shows a decrease with increasing overheat. This is also an effect of reduced wall viscosity, as predicted by the theory. Flush-mounted hot-film anemometer data show no dependence of the boundary layer intermittency upon azimuthal angle, even at overheats above 15 °C. If one of the three possible buoyancy-driven instabilities were dominant, then transition should tend to occur first on either the top, bottom, or side wall.

We can conclude from these results that buoyancy effects probably do not explain the departures of flow-tube transition Reynolds numbers from theoretical predictions. Most of the buoyancy measurements were performed at lower flow velocities than those used to measure transition Reynolds numbers, because at low velocities the buoyancy effects should be most apparent. Presumably if the flow tube were made sufficiently longer, these effects would become significant.

3.6. *Effect of water purity upon reproducibility*

The highest transition Reynolds numbers, as presented in figure 5, can be obtained only under ideal experimental conditions. Although these 'best' results have been repeated more than once, there have been many experimental runs in which lower transition Reynolds numbers were obtained. In some cases the lower Reynolds numbers were found to be caused by some defect in the apparatus, such as a broken screen wire or a malfunctioning heater. However, most of the scatter in transition Reynolds-number data can be attributed to variations in the free stream particulate content. The water supply purity varies considerably with weather conditions at the site, and these changes in purity are directly correlated with changes in transition Reynolds number. Under the most adverse conditions, this effect has reduced the maximum transition Reynolds number with heat to less than 20 million. However,

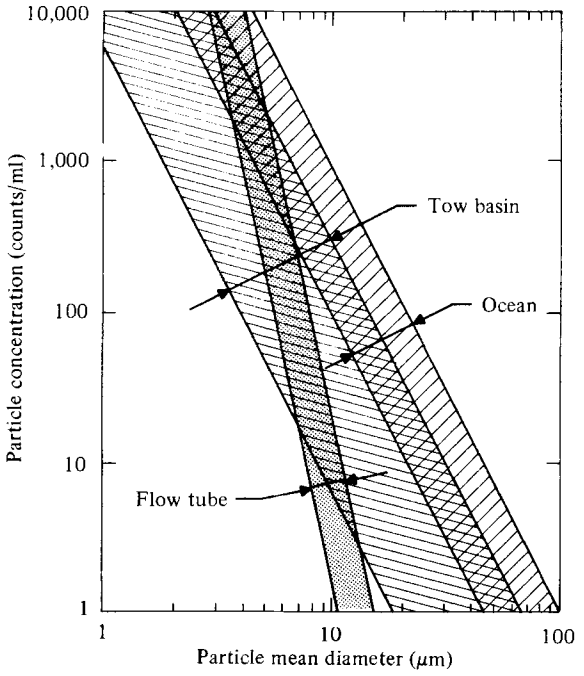

FIGURE 12. Particle concentration spectra: flow tube, ocean water, and NSRDC towing basin.

if we compare only results obtained during periods of known high water purity, the standard deviation of the Reynolds numbers is less than 10 % of the mean.

This high sensitivity to relatively low levels of free-stream particulate content was quite unexpected. Considerable effort has been made to improve the water quality by in-line filtering upstream of the settling chamber. A two-metre diameter filtration tank was added to the supply pipeline. In addition, frequent measurements of the particle concentration spectrum have been made with a Coulter counter (model ZH). The range of the particle spectrum results is shown in figure 12. Also shown in this figure are the spectrum ranges for the ocean and for the NSRDC towing basin (Bethesda, Maryland). Note that the flow tube particle spectrum has a steeper downward slope than either of the other two. This implies that for particle sizes greater than 10 μm, which are outside of the Coulter counter range, the flow tube may be much cleaner than the other two sources. Although the mechanism by which particulate contamination influences transition is not known at present, it seems likely that particles smaller than 10 μm are not important. The filtration system used in this experiment effectively removes all particles larger than 100 microns. Whatever the mechanism of interaction with the boundary layer, it is clear that contamination effects should be carefully considered in any future research on wall heat stabilization.

4. Conclusions

The flow tube experiment has shown that wall heating can have a significant stabilizing effect upon water boundary layers. Theoretical predictions of this effect appear to be nearly correct at overheats of less than 8 °C. The flow tube has achieved a maximum transition Reynolds number of 47·5 million with 8 °C overheat. This can be compared with a value of 15 million with no heat, or a value of 5 million in a previous flow tube experiment in air (Wells 1967; Spangler & Wells 1968).

At wall overheats higher than 8 °C, the experiment yields no further increases in transition Reynolds number, while the theory predicts additional increases up to an overheat of 35 °C. Possible causes of this discrepancy include the effects of buoyancy, wall roughness, and differences between the theoretical and experimental flow geometries. An unexpected sensitivity to very small concentrations of suspended particulate matter in the free stream has also been observed. Additional studies in the flow tube have shown that the disagreement between theory and experiment probably cannot be attributed to the effects of buoyancy or geometric differences. A detailed parametric study of the effects of wall roughness in heat-stabilized boundary layers is needed. Furthermore, approximations made in the theory, such as the e^9 criterion for transition, should be questioned.

Velocity measurements in the flow tube have discovered the presence of azimuthal variations in boundary layer thickness, which appear to be the result of streamwise vorticity in the boundary layer. The origin of these vortices is not known, but the experiment has shown that they are not generated by turbulence manipulators in the settling chamber or by a Goertler instability in the contraction. Similar three-dimensional disturbances have been observed by other researchers in high Reynolds number laminar boundary layers.

The authors wish to acknowledge the support of the Defence Advanced Research Projects Agency, and in particular Dr Philip Selwyn and Dr George Donohue. We also acknowledge the contributions of Colorado State University, Dynamics Technology, Inc., and Professor Eli Reshotko of Case Western Reserve University.

Some of the results in this paper have also been presented at the ONR Twelfth Symposium on Naval Hydrodynamics, Washington, D.C., 1978.

REFERENCES

BACK, L. H., CUFFEL, R. F. & MASSIER, P. F. 1969 *A.I.A.A. J.* **7**, No. 4, 730.

BARKER, S. J. & JENNINGS, C. 1977 The effect of wall heating on transition in water boundary layers, *Proc. of NATO-AGARD Symp. on Laminar-Turbulent Transition*, Copenhagen, p. 19–1.

BARKER, S. J. 1978 Turbulence management in a high-speed water flow facility *A.S.M.E.*

BRADSHAW, P. 1965 The effect of wind tunnel screens on nominally two-dimensional boundary layers. *J. Fluid Mech.* **22**, 679.

CHMIELEWSKI, G. E. 1974 *J. Aircraft* **11**, 436.

CORRSIN, S. 1963 Turbulence: Experimental methods. In *Handbuch der Physik*, vol. 8, p. 523.

KAUPS, K. & SMITH, A. M. O. 1967 The laminar boundary layer in water with variable properties. *Proc. ASME-AIChE Heat Transfer Conf., Seattle, Washington.*

LAUNDER, B. E. 1964 Laminarization of the turbulent boundary layer by acceleration, *M.I.T. Gas Turbine Lab Report* 77.

LOEHRKE, R. I. & NAGIB, H. M. 1972 Experiments on management of free-stream turbulence, *NATO-AGARD Rep.* 598.

LUMLEY, J. L. & MCMAHON, J. F. 1967 *Trans. A.S.M.E.* D, *J. Basic Engng* **89**, 764.

PANKHURST, R. C. & HOLDER, D. W. 1954 *Wind Tunnel Technique.* Pitman.

SCHLICHTING, H. 1968 *Boundary Layer Theory.* McGraw-Hill.

SMITH, A. M. O. 1957 Transition, pressure gradient, and stability theory, *Proc. 9th Int. Congress on Appl. Mech., Brussels*, vol. 4, 234.

SPANGLER, J. G. & WELLS, C. S. 1968 *A.I.A.A. J.* **6**, 543.

STRAZISAR, A. J., PRAHL & RESHOTKO, E. 1977 Stability of heated laminar boundary layers in water, *Proc. NATO-AGARD Symposium on Laminar-Turbulent Transition*, Copenhagen.

WAZZAN, A. R., OKAMURA, T. T. & SMITH, A. M. O. 1968 *Trans. A.S.M.E.* C, *J. Heat Transfer* **90**, 109.

WAZZAN, A. R., OKAMURA, T. T. & SMITH, A. M. O. 1970 The stability and transition of heated and cooled incompressible boundary layers. *Proc. 4th Int. Heat Transfer Conf., Paris.*

WELLS, C. S. 1967 *A.I.A.A. J.* **5**, 172.

WILSON, S. D. R. & GLADWELL, I. 1978 The stability of a two-dimensional stagnation flow to three-dimensional disturbances. *J. Fluid Mech.* **84**, 517.